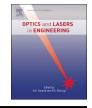


Contents lists available at ScienceDirect

Optics and Lasers in Engineering



journal homepage: www.elsevier.com/locate/optlaseng

## Assessment of speckle-pattern quality in digital image correlation based on gray intensity and speckle morphology



Jihyuk Park<sup>a</sup>, Sungsik Yoon<sup>a</sup>, Tae-Hyun Kwon<sup>b</sup>, Kyoungsoo Park<sup>a,\*</sup>

<sup>a</sup> Department of Civil and Environmental Engineering, Yonsei University, 50 Yonsei-ro, Seodaemun-gu, Seoul 120-749, Republic of Korea <sup>b</sup> Korea Atomic Energy Research Institute, 989-111 Daedeok-daero, Yuseong-gu, Daejeon 305-353, Republic of Korea

#### ARTICLE INFO

Keywords: Speckle-pattern quality Digital image correlation Deformation measurement Gray intensity Speckle morphology

### ABSTRACT

In digital image correlation (DIC), speckle patterns are generated on the surface of a specimen to resolve uniqueness issues. Thus, speckle patterns significantly affect the accuracy of image correlation. To assess the quality of speckle patterns, the standard deviation of grav intensities within each speckle (SDGIS) is introduced as a new metric. On the basis of the cumulative distribution of SDGIS, speckle-pattern quality measurement ( $\rho$ ) is proposed, which integrates the features of gray intensity and speckle morphology. Twelve speckle patterns are generated by changing the spraying time and nozzle sizes of an airbrush because these are associated with the speckle volume fraction and speckle size, respectively. In addition, three displacement fields are used to investigate the effects of speckle patterns on the accuracy of the DIC results. For the 12 speckle images associated with the three displacement fields, the correlation results demonstrate that the proposed specklepattern quality measurement is inversely proportional to the averaged error of the subset method. This is statistically confirmed by evaluating the correlation coefficient and p-value. Furthermore, the error of the subset method is more affected by speckle patterns than the subset size when the subset size is sufficiently large.

#### 1. Introduction

Digital image correlation (DIC) is an effective optical technique used to measure surface deformation in the field of experimental mechanics. Owing to the rapid advances in optical and computer vision technologies, DIC has been extensively employed in various engineering applications [22,30]. For example, DIC techniques were employed to investigate various material properties, such as those of metals [2,26], brittle materials [1,11,18], quasi-brittle materials [7,27], thin films [15], interfacial debonding [5], biological materials [35], and others.

To improve the accuracy of optical measurements, several imagecorrelation algorithms were developed [16,29,6]. For example, a linear approximation of a deformation map was extensively used [29,31,4]. Subsequently, Lu and Cary [16] introduced mapping parameters in conjunction with the second-order Taylor series approximation of a displacement field. To provide compatibility requirements among subset deformations, Cheng et al. [6] developed a full-field image correlation using the B-spline deformation function. In addition, Poissant and Barthelat [25] extended the subset method to account for a discontinuous displacement field by employing a subset-splitting procedure. Pan et al. [24] modified the subset-based method to

measure the displacement of arbitrary shapes of selected regions of interest. Cofaru et al. [8] proposed an adaptive image-correlation technique by specifying subsets as irregular shapes in conjunction with speckle patterns. Recently, Yuan et al. [34] has automatically determined the subset size in relation to the necessary amount of speckle information.

For accurate estimation of a strain field, a displacement field is smoothened by employing several techniques [17,21,22,28,32]. For instance, Sutton et al. [28] proposed to smoothen a computed displacement field using a penalty finite element method, whereas Meng et al. [17] utilized the finite element method and a generalized cross-validation algorithm. Wattrisse et al. [32] and Pan et al. [21] employed a local least-square fitting technique to filter noisy displacement data.

Furthermore, speckle patterns significantly affect the accuracy of the correlation results because they are associated with their uniqueness. Thus, the evaluation of the speckle-pattern quality is one of the essential aspects in DIC. Previously, speckle patterns were assessed using several metrics in terms of the gray-level intensities or morphological features. For example, a subset entropy [33] and a mean subset fluctuation [12] were defined according to the differences in the gray intensities among adjacent pixels. Pan et al. [20,23] utilized a sum-of-

E-mail address: k-park@yonsei.ac.kr (K. Park).

http://dx.doi.org/10.1016/j.optlaseng.2016.11.001

Received 23 February 2016; Received in revised form 18 October 2016; Accepted 5 November 2016 Available online 18 November 2016

0143-8166/ © 2016 Elsevier Ltd. All rights reserved.

<sup>\*</sup> Corresponding author.

square subset intensity gradient and a mean intensity gradient for quality assessment of speckle patterns. In addition, Fazzini et al. [10] investigated the effects of image encoding and image saturation on the correlation error. However, numerically generated synthetic patterns were utilized, instead of actual speckle patterns, in all the aforementioned metrics. Moreover, the morphological features of synthetic patterns may be different from those generated by an airbrush.

To account for the local morphological features in speckle patterns, Lecompte et al. [14] estimated the size of speckle patterns by converting a gray-scale image to a binary image and calculated the cumulative percentage of the speckle sizes. We note that they generated a single speckle pattern and obtained three different speckle sizes using images generated at three different distances. Crammond et al. [9] also evaluated the cumulative percentage of speckle sizes for two types of speckle patterns: a) speckle patterns generated by an airbrush and b) speckle patterns generated by spray painting. However, in actual experiments, various speckle patterns can be generated by changing the experimental conditions such as nozzle sizes, air pressure, spraying distance, airbrush conditions, and others. Furthermore, none of the previous studies showed a direct relationship between the DIC error and quality assessment of speckle patterns. In this context, a metric, which represents the quality of speckle patterns, should be based on both gray-level intensity and local morphological features and be valid under various experimental conditions.

In the present study, various speckle patterns are quantified by introducing a speckle-pattern quality measurement  $(\rho)$  based on the standard deviation of gray intensities within each speckle (SDGIS). We note that SDGIS accounts for both gray-level intensity and speckle morphology. To confirm the consistency of the proposed measurement, various speckle patterns are first generated by changing the spraying time and nozzle sizes of an airbrush, which leads to the variation in the speckle volume fraction and speckle sizes. For such speckle patterns, the DIC results demonstrate that the values of  $\rho$  are inversely proportional to the averaged errors of the DIC. The remainder of this paper is organized as follows. Section 2 briefly explains the DIC principle. In Section 3, various speckle patterns generated by changing the spraying time and nozzle sizes are presented. Quantification of the generated speckle patterns based on SDGIS is discussed in Section 4. Section 5 demonstrates three computational experiments, i.e., uniaxial compression, three-point bending, and mode-I fracture, for the generated and quantified speckle patterns as well as the subsequent statistical estimation of the relationship between  $\rho$  and the averaged DIC error. Finally, the key findings of this study are summarized in Section 6.

#### 2. DIC principle

In DIC, the gray intensity of a reference image is compared with that of a deformed image. We note that a reference image corresponds to an undeformed state of a deformed image. In the present study, the displacement field within a region of interest is evaluated using the subset method with a second-order approximation of the displacement field [16].

The gray-level intensity of each subset in a reference image is correlated to the gray-level intensity of each subset in a deformed image. A subset in a reference image is generally selected as a square with a size of (2m+1) by (2m+1) pixels, where *m* is an integer. Given that point  $(x_n, y_n)$  of the *n*th subset in a reference image is displaced at point  $(\bar{x}_n, \bar{y}_n)$  in the *n*th subset of a deformed image, as shown in Fig. 1, we can obtain the following relationships:

$$\overline{x_n} = x_n + u_n \tag{1}$$

 $\overline{y_n} = y_n + v_n \tag{2}$ 

where  $u_n$  and  $v_n$  are the horizontal and vertical displacement fields, respectively, of a point in the *n*th subset. The horizontal and vertical

displacement fields are approximated by employing the second-order Taylor series expansion around the origin of the local coordinates ( $\xi$ ,  $\eta$ ) of a subset [16]. These are expressed as

$$u_n(\xi,\eta) \approx u_{n0} + \frac{\partial u_{n0}}{\partial \xi} \xi + \frac{\partial u_{n0}}{\partial \eta} \eta + \frac{1}{2} \frac{\partial u_{n0}}{\partial \xi} \xi^2 + \frac{1}{2} \frac{\partial u_{n0}}{\partial \eta} \eta^2 + \frac{\partial u_{n0}}{\partial \xi \partial \eta} \xi \eta$$
(3)

$$v_n(\xi,\eta) \approx v_{n0} + \frac{\partial v_{n0}}{\partial \xi} \xi + \frac{\partial v_{n0}}{\partial \eta} \eta + \frac{1}{2} \frac{\partial v_{n0}}{\partial \xi} \xi^2 + \frac{1}{2} \frac{\partial v_{n0}}{\partial \eta} \eta^2 + \frac{\partial v_{n0}}{\partial \xi \partial \eta} \xi \eta \tag{4}$$

where  $u_{n0}$  and  $v_{n0}$  are the horizontal and vertical displacements, respectively, at  $\xi=0$  and  $\eta=0$ , i.e., the displacements of the center (or grid) point of a subset.

The horizontal and vertical displacements of the grid points are evaluated by minimizing the square of the gray-level intensity difference  $(\Psi_n)$  of the *n*th subset between a reference image and a deformed image, i.e.,

$$\min \Psi_n = \min \frac{\sum_{i=1}^{n_{px}} [I_r(p_i) - I_d(p_i, \lambda_n)]^2}{\sum_{i=1}^{n_{px}} I_r^2(p_i)}$$
(5)

where  $n_{px}$  is the number of pixels in the *n*th subset of a reference image [i.e.,  $n_{px}=(2m+1)^2$ ]. We note that  $I_r(p_i)$  is the gray-level intensity of the *i*th pixel  $(p_i)$  in the reference image, whereas  $I_d(p_i, \lambda_n)$  is the gray-level intensity of the *i*th pixel  $(p_i)$  in the deformed image. The gray-level intensity  $(I_{cl})$  in the deformed image is evaluated using the bicubic spline interpolation.

$$I_d(p_i, \lambda_n) = \sum_{s=0}^{3} \sum_{t=0}^{3} \beta_{st} (\bar{x}_n - x_p)^s (\bar{y}_n - y_p)^t + \chi$$
(6)

where  $x_p$  and  $y_p$  are the nearest pixel position of  $(\bar{x}_n, \bar{y}_n)$ , respectively, in the deformed image and  $\beta_{st}$  is the fitting coefficient obtained from the adjacent gray-level intensities. In addition, a gray-level intensity offset ( $\chi$ ) is considered between the reference and deformed images due to changes in the light. The vector of the mapping parameters ( $\lambda_n$ ) consists of a gray-level intensity offset and 12 coefficients from the second-order Taylor series expansion.

#### 3. Generation of speckle patterns

Various speckle patterns are generated by changing the volume fraction and speckle sizes. The volume fraction is addressed by changing the spraying time, whereas the various speckle sizes are obtained by changing the nozzle sizes of an airbrush. After generating various speckle patterns, images of the speckle patterns are obtained using a camera (in this instance, a Canon EOS 5D Mark II). The focal length and object distance are 180 mm and 0.54 m, respectively, with a pixel size of 8.5  $\mu$ m.

In this study, three speckle volume fractions (i.e., low, medium, and high) are employed with respect to four nozzle sizes of 0.2, 0.5, 1.0, and 1.2 mm, which lead to 12 cases of speckle patterns. To calculate the speckle volume fraction, the image of the random speckle patterns is converted to a binary image, which consists of black and white, according to the threshold of the grav-level intensity. We note that the threshold is selected by maximizing a discriminant measurement, known as the Otsu method [19]. The calculated volume fractions of the 12 cases of speckle patterns with an image size of 3000×3000 pixels are listed in Table 1. Fig. 2 shows the speckle patterns and their binary images for the regions of interest spanning 100×100 pixels with a nozzle size of 1.0 mm according to the change in the speckle volume fraction. For longer spraying times, the small speckles are merged, and relatively larger speckles are generated, which result in the appearance of darker areas, i.e., higher volume fractions. Fig. 3 shows that the increase in the nozzle size leads to larger speckle sizes, as expected, when the speckle volume fraction is in the medium range.

The combinations of the three volume fractions and four nozzle sizes lead to various gray-level intensity distributions within an image.

Download English Version:

# https://daneshyari.com/en/article/5007870

Download Persian Version:

https://daneshyari.com/article/5007870

Daneshyari.com